47691-6001-UT-00

Microwave Scattering from Internal Wave Modulated Surface Waves: A Shipboard Real Aperture Coherent Radar Study in JOWIP (The Georgia Strait Experiment)

by

D. S. W. Kwoh
B. M. Lake
H. Rungaldier

26 June 1988

Prepared for

Office of Naval Research
Contract No. N00014-86-C-0111

TRW Space & Technology Group
One Space Park
Redondo Beach, California 90278

UNCLASSIFIED

SECURITY CLASSIFICATION OF THIS PAGE

REPORT DOCUMENTATION PAGE

1a. REPORT SECURITY CLASSIFICATION UNCLASSIFIED	1b. RESTRICTIVE MARKINGS
2a. SECURITY CLASSIFICATION AUTHORITY	3. DISTRIBUTION/AVAILABILITY OF REPORT Approved for public release, distribution unlimited
2b. DECLASSIFICATION/DOWNGRADING SCHEDULE	
4. PERFORMING ORGANIZATION REPORT NUMBER(S) 47691-6001-UT-00	5. MONITORING ORGANIZATION REPORT NUMBER(S)
6a. NAME OF PERFORMING ORGANIZATION Fluid Mechanics Department TRW Space & Technology Group 6b. OFFICE SYMBOL (If applicable)	7a. NAME OF MONITORING ORGANIZATION
6c. ADDRESS (City, State, and ZIP Code) One Space Park Redondo Beach, California 90278	7b. ADDRESS (City, State, and ZIP Code)
8a. NAME OF FUNDING/SPONSORING ORGANIZATION Office of Naval Research 8b. OFFICE SYMBOL (If applicable)	9. PROCUREMENT INSTRUMENT IDENTIFICATION NUMBER
8c. ADDRESS (City, State, and ZIP Code) Department of the Navy 800 North Quincy Street Arlington, VA 22217-5000	10. SOURCE OF FUNDING NUMBERS PROGRAM ELEMENT NO. / PROJECT NO. / TASK NO. / WORK UNIT ACCESSION NO.

11. TITLE (Include Security Classification)
Microwave Scattering from Internal Wave Modulated Surface Waves: A Shipboard Real Aperture Coherent Radar Study in JOWIP (The Georgia Strait Experiment)

12. PERSONAL AUTHOR(S)
D. S. W. Kwoh, B. M. Lake, H. Rungaldier

13a. TYPE OF REPORT	13b. TIME COVERED	14. DATE OF REPORT (Year, Month, Day)	15. PAGE COUNT
Final (1 of 2)	FROM 1/1/86 TO 6/27/88	June 27, 1988	50

16. SUPPLEMENTARY NOTATION

17. COSATI CODES			18. SUBJECT TERMS (Continue on reverse if necessary and identify by block number)
FIELD	GROUP	SUB-GROUP	Internal Waves, Surface Wave Modulations, Georgia Strait Experiment

19. ABSTRACT (Continue on reverse if necessary and identify by block number)

A shipboard cw coherent dual-polarized focused radar operating at 9.23 GHz and an optical device which detects the occurrence of specular reflection at the radar incidence angle have been used to investigate mechanisms governing radar backscatter from surface water waves as part of JOWIP (The Georgia Strait Experiment). The relative contributions of Bragg and specular backscatter mechanisms have been identified using the output of the optical specular detector and the radar backscatter polarization ratios. Analysis of the radar data together with data from the DREP laser wave slope gauge (Hughes and Dawson, this issue) has been used to further identify the mechanisms governing radar backscatter and modulations of radar backscatter from surface water waves. It is found that specular reflection is very significant at 20° incidence angle and not negligible at 40°. It is found that when specular contributions are absent the relationship between the surface wave slope and the radar backscatter is well-described by Bragg theory. Specular contributions, when they
(Cont. on back of this page)

20. DISTRIBUTION/AVAILABILITY OF ABSTRACT	21. ABSTRACT SECURITY CLASSIFICATION
☐ UNCLASSIFIED/UNLIMITED ☒ SAME AS RPT. ☐ DTIC USERS	UNCLASSIFIED
22a. NAME OF RESPONSIBLE INDIVIDUAL	22b. TELEPHONE (Include Area Code) / 22c. OFFICE SYMBOL

DD FORM 1473, 84 MAR 83 APR edition may be used until exhausted. All other editions are obsolete.

SECURITY CLASSIFICATION OF THIS PAGE
UNCLASSIFIED

occur, appear as large spikes on top of the Bragg return. Analysis of the wave slope data shows that the wave slope modulations at "X-band" and "L-band" Bragg wave frequencies are comparable, in contradiction to standard wave modulation theories which predict that "X-band" waves should exhibit much weaker modulations. Modulations of the radar backscatter in calm seas are due primarily to Bragg scattering. As the wind speed increases, the hydrodynamic modulations tend to decrease but the radar modulations can be enhanced by specular reflection. Possible additional contributions due to wedge-diffraction-type scattering at higher wind speeds have not been addressed in this experiment. Deep minima, which may be due to the presence of organic films on the surface, have been observed in some radar returns near current patterns.

ABSTRACT

A shipboard cw coherent dual-polarized focused radar operating at 9.23 GHz and an optical device which detects the occurrence of specular reflection at the radar incidence angle have been used to investigate mechanisms governing radar backscatter from surface water waves as part of JOWIP (The Georgia Strait Experiment). The relative contributions of Bragg and specular backscatter mechanisms have been identified using the output of the optical specular detector and the radar backscatter polarization ratios. Analysis of the radar data together with data from the DREP laser wave slope gauge (Hughes and Dawson, this issue) has been used to further identify the mechanisms governing radar backscatter and modulations of radar backscatter from surface water waves. It is found that specular reflection is very significant at 20° incidence angle and not negligible at 40°. It is found that when specular contributions are absent the relationship between the surface wave slope and the radar backscatter is well-described by Bragg theory. Specular contributions, when they occur, appear as large spikes on top of the Bragg return. Analysis of the wave slope data shows that the wave slope modulations at "X-band" and "L-band" Bragg wave frequencies are comparable, in contradiction to standard wave modulation theories which predict that "X-band" waves should exhibit much weaker modulations. Modulations of the radar backscatter in calm

seas are due primarily to Bragg scattering. As the wind speed increases, the hydrodynamic modulations tend to decrease but the radar modulations can be enhanced by specular reflection. Possible additional contributions due to wedge-diffraction-type scattering at higher wind speeds have not been addressed in this experiment. Deep minima, which may be due to the presence of organic films on the surface, have been observed in some radar returns near current patterns.

MICROWAVE SCATTERING FROM INTERNAL WAVE MODULATED SURFACE WAVES: A SHIPBOARD REAL APERTURE COHERENT RADAR STUDY IN JOWIP (THE GEORGIA STRAIT EXPERIMENT)

1. INTRODUCTION

During JOWIP (The Georgia Strait Experiment), synthetic aperture radar (SAR) imaging of internal waves was investigated by obtaining SAR images of internal waves at X- and L-bands while a variety of surface and subsurface measurements were being made to provide quantitative data on each of the mechanisms linking internal wave displacements to SAR image intensity variations (see Hughes and Dawson, this issue). In particular, measurements were made of surface currents, surface wave slopes, real aperture X-band backscatter from a shipboard radar, the occurrence of specular facets (at the radar incidence angles) on the water surface, and meteorological data such as wind speed and direction. TRW provided the shipboard X-band radar and a video system for detection of specular facets. This paper describes the equipment, the measurements, and how the data has been used together with the wave slope data to identify the mechanisms responsible for radar backscatter and backscatter modulations.

The shipboard X-band radar was deployed with the following two objectives:

(i) To determine the importance of specular reflection at 20° and 40° incidence angles by using a video camera to

detect the presence of specular facets while microwave scattering is taking place.

(ii) To test scattering models by measuring the in-situ X-band backscattering cross-section of the ocean and comparing the cross-section modulation with the output of the laser slope gauge (deployed by B. Hughes of the Defense Research Establishment of the Pacific, or DREP).

Measurements to address the above two objectives were made for both ambient wind wave conditions and wind waves which were undergoing modulations by internal waves.

2. EXPERIMENT DESCRIPTION

Equipment. The radar except for minor modifications, is the same unit that we have used in previous laboratory wave tank-wind tunnel scattering studies.[1,2] It is an X-band CW dual-polarized system, operating at 9.13 GHz with roughly 1 watt output. The antenna is a 22.9 cm aperture conical corrugated horn with a matched dielectric lens for spot focusing. The 3 dB (2 way) spot size is 18 cm at the 1 m focal plane. The radar is a superheterodyne system, with the transmitter frequency offset from the local oscillator frequency by 30 MHz. Each polarization channel (vv or hh) has two modes of output. The "raw data" mode is simply the 30 MHz IF signal downconverted to 20 KHz. This signal can be used for accurate power measurement and Doppler spectrum analysis. The "processed data" mode has separate linear

amplitude (i.e., not power) and phase (-180° to +180°) output channels for chart display.

For detecting specular points, a bright diffused light, consisting of an aircraft landing light with a diffuser in front, is mounted on one side of the horn antenna and a video camera is mounted on the other side. Both are pointed at the focal spot of the horn on the water surface. A drawing showing the mounting arrangement is shown in Figure 1.

The horn, lamp and video camera were mounted onto the frame of DREP's laser slope gauge onboard the CFAV Endeavour, with a distance of roughly 1 m from the water surface. The incidence angle of 20° or 40° was set at the beginning of the day. The horn and video equipment were always pointed along the axis of the ship.

On the bow of the ship was mounted a separate video camera for recording the general features of the wave field the ship was going through.

Data from the radar unit, the time code generator, as well as from some DREP equipment (such as the laser slope gauge, current meter, wind meter, wave height gauge) were recorded on two analog recorders. The two video cameras' outputs were recorded on two video recorders.

Data collected consists of 119 runs, each run being a more or less continuous recording ranging from a minute to more than 1/2 hour. For natural internal waves, there are

66 runs of which 36 have SAR overpasses. Roughly 82% of the runs have good data.

Procedures. Each morning, calibration and alignment were carried out on the deck of the Endeavour before the equipment was lowered close to the water surface. Alignment of the lamp and video camera with the focal spot of the horn was first checked with the help of a template mounted at the horn's focal plane. The incidence angle for the day was then set relative to DREP's slope gauge axis. A metallic sphere was then swung through the focal plane of the horn to calibrate the radar unit. After the equipment was lowered into position, the height above the water surface was visually checked from the bow and adjusted accordingly.

The only experimental difficulty we have encountered was the almost constant tuning that was required for the radar. In a laboratory environment, once the radar unit was tuned to null away stray reflections, it would stay tuned for hours. In the ocean, the horn antenna was mounted onto the DREP slope gauge which swayed slightly from side to side when going through a wave field. Since the horn was connected via two 28' waveguides to the radar unit, the swaying motion induced phase changes in the return signal, effectively detuning it continuously. In a rough sea at a 20° incidence angle, the backscattered signal is much stronger than this detuning noise. In a calm sea at a 40° incidence angle, the signal/detuning noise ratio could become quite severe. Fortunately, our receiver has an IF

output which records the raw signal down converted to 20 kHz. When this IF signal is down converted to 40 Hz, detuning appears as a sharp peak at 40 Hz, distinct from the real backscattered signal, which is usually Doppler shifted by ten's of Hz from 40 Hz.

3. RESULTS OF SPECULAR REFLECTION MEASUREMENTS

Specular reflection occurs when a point on the water surface has its surface normal pointing directly in the microwave incidence direction. When this occurs, backscattered power increases drastically for a short duration so that the output is like a spike. By its nature, specular reflection has no polarization dependence (in contrast to Bragg scattering), so that vv and hh scattering have equal power*. These two characteristics can be used to identify specular reflection events in microwave backscattering. For positive identification of specular reflection, however, we have to rely upon the coincidence of bright patches or dots on the video monitor with spikes in the microwave backscattered power. Figure 2 shows an example of this. The top row shows three different pictures on the TV monitor at three different times. It can be seen that the presence of bright dots or patches coincides with occurrence of high outputs (spikes) in both the vv and hh channel. Furthermore, vv and hh have the same power level in the spikes. Between the two specular events there are

*Where vv and hh refer to the polarization states: vv is vertical transmit-vertical receive and hh is horizontal transmit-horizontal receive.

nonspecular events where vv amplitude is roughly twice that of hh, as expected from Bragg scattering at 40° incidence angle.

Traces 3 and 4 show DREP's slope and wave height measurement for the same time period. The occurrence of specular events cannot be inferred in any way from these traces. One reason for this, of course, is that slope and wave height gauges are not co-located but are about 0.7 m away from the radar antenna footprint. The major reason, however, is that the slope and wave height measurements are point measurements whereas the radar backscattering is an area measurement. For detecting an event which is small in spatial extent and short in time, such as the specular facet, an area measurement will show a much higher frequency of detection than a point measurement. Suppose r_a = radius of radar antenna footprint, r_{sp} = radius of curvature of specular point, r_ℓ = radius of laser beam on the water surface. If $r_a \gg r_{sp} \gg r_\ell$, it is easy to show that

$$\frac{\text{probability of detecting a specular point by laser beam}}{\text{probability of detecting a specular event by radar}} \approx \left(\frac{r_{sp}}{r_\ell}\right)^2$$

Since the 10 dB radius of the antenna = 15 cm, the specular point radius of curvature typically ≃ a few mm and the laser beam radius ~ 0 (1 mm), the above probability ratio

$$\simeq 0\left(\frac{0.5}{15}\right)^2 \simeq 0(900).$$

This is the reason why the specular reflection events detected by the radar can only be correlated with the video recording (an area measurement) rather than the slope gauge or wave-height gauge.

To determine the amount of specular reflection under different sea states and incidence angles, we use the following setup. The video tape containing the video camera recording is replayed onto a TV monitor. A camera with a photodiode in its film plane views the TV monitor continuously. The photodiode output will show spikes whenever a bright patch or dot appears on the TV screen. The spikes occur in groups and within the groups they are roughly 1/60 sec apart, 1/60 sec being the TV field rate. The magnitude of each spike is proportional to the magnitude of the specular return. The analog tape containing the microwave data is also replayed simultaneously. If the video tape and the analog tape are synched correctly, the photodiode output spikes should coincide with a specular event in the microwave channel. Since both video recorder and analog recorder are mechanical devices, synching both to the accuracy involved (1/10 sec) over a long period of time is almost impossible. We solved this problem by inputting both photodiode output and the microwave data into a digital scope with large memory. Proper synching is then performed on the digital scope. Using this method, roughly 10 minutes of data can be analyzed at a stretch. For each continuous segment of data, the total amount of power due to specular reflection as well as the total time during which specular reflection occurs are summed. (We are assuming for simplicity that whenever the video camera sees bright dots and patches, the corresponding microwave power comes from

specular reflection.) These are then expressed as a fraction of the total power and a fraction of the total time of the data segment. The results as a function of wind speed and incidence angle are shown in Figures 3 and 4. In order to obtain as statistically meaningful a set of results as possible, about 52 minutes of data were processed from a total of 21 runs covering a range of wind speeds from 0.7 to 8.6 m/sec and two incidence angles (20° and 40°). Except for the cases as indicated, all the data points are from pure wind wave runs, i.e., where internal waves are absent. In all cases, the ship is sailing directly into the wind ±30°. From the figures, we can draw the following conclusions:

(i) For 20° incidence, specular power as a fraction of total power varies from ~70% at low wind (~ 1 m/s) to 90% at high wind (~ 8 m/s).

(ii) For 40° incidence, specular power increases from almost nothing at low wind to ~ 30-40% at 7 m/s.

(iii) For 20° incidence, the time during which specular reflection occurs is ~ 20% of the total time.

(iv) At 40° incidence, the presence of an internal wave field increases power in specular reflection quite noticeably. This probably is a result of enhanced induced "wavebreaking" by the internal wave.

We want to point out that the above conclusions are from data sets obtained in Dabob Bay and Boundary Pass where the fetch is highly limited. It does show, however, that

specular reflection at X-band is more significant than has been generally expected. It has generally been assumed that specular contributions should be negligible at incidence angles greater than 20° (see, e.g., Valenzuela, 1978).

An often heard comment discounting the possible importance of specular reflection at X-band is that "facets on the water surface which are optically specular may not be specular to microwave radiation". The exact meaning of this statement is that the radius of curvature at the specular points may be much smaller than the microwave wavelength (but would still be much longer than optical wavelength). In this case, microwave scattering from the specular points would be Rayleigh scattering, i.e.,

$$\sigma_{microwave} \propto \pi r^2 (kr)^4$$

where r = radius of curvature at specular point

$k = 2\pi/\lambda$

λ = microwave wavelength

For optical wavelengths, scattering would be in the geometric optics region so that cross section would be given by

$$\sigma_{optical} \doteq \pi r^2$$

Thus, if $r \ll \lambda$, $(kr)^4$ will be $\ll 1$ and $\sigma_{microwave} \ll \sigma_{optical}$.

To answer the question whether specular reflection at X- and L-bands is predominantly Rayleigh scattering, we need to know the size distribution of the specular facets (or,

more accurately, the radius of curvature distribution of the specular points). This can be estimated by analyzing the video images we have recorded. Since our illumination source is a finite size diffused lamp, the apparent size of the image of the lamp in water at each specular point will be directly related to the radius of curvature at that specular point (see Appendix A). This analysis has been carried out for two wind wave runs at 40° incidence. Figure 5 shows the size distribution of the facets for one run plotted as histograms in kr for both X- and L-bands. Generally speaking, $kr < 1$ can be regarded as the Rayleigh scattering region, $1 < kr < O(10)$ can be regarded as the resonance region and $kr > O(10)$ can be regarded as the geometric optics region. Blooming on the TV screen may be a significant source of error in measuring the size of small facets.

Figure 6 shows power distribution of the facets plotted as histograms in kr, i.e., the vertical axis shows total power contributed by facets of each particular kr value. It can be seen that for X-band, most of the specular reflection occurs in the resonance and geometric optics region, i.e., the facets are not small relative to the X-band wavelength at 40° incidence. For L-band, there is more Rayleigh scattering but still most of the specularly reflected power occurs in the resonance region and geometric optics region. Our measurements may be subject to errors due to blooming (as mentioned above) and motion blurring. Blooming may

impose a lower limit on size measurement. Its error for big patches should be much smaller in proportion. We have calibrations giving us a rough estimate of the error due to blooming. For motion blurring, the correct solution (which may be implemented in future tests) should be the use of either a fast shutter in front of the video camera or a synchronized flash lamp. For our recorded data, we can measure only the cross-track size of the patches. This presumably is not subject to motion blurring. With all these caveats, we think it is still safe to conclude that at X-band at 40° incidence, specular reflection occurs principally in the resonance and geometric optics region.

The relative contributions of specular and Bragg backscatter to the total return as a function of the size of the radar illumination spot on the water surface has not been investigated in these experiments. A question can be raised as to how the relative contributions might vary as platform altitude and/or spot size is varied. Specular contributions would add incoherently and might be overwhelmed by Bragg contributions which would increase faster than linearly if they continued to add coherently. Since water waves at centimeter scales are expected to have correlation scales of no more than a few of their own wavelengths, we expect that as the illumination spot is increased over that used in this experiment, the contributions from both Bragg and specular mechanisms will add incoherently and the relative contributions should be

close to what we have observed here even for platforms at much higher altitudes. We intend to investigate this aspect of the problem quantitatively in future experiments. We wish to emphasize that the video system was meant from the beginning to detect specular points. It was only after the data had been collected that we realized some semi-quantitative information could be gathered about specular reflection in general and about the radii of curvature of specular points in particular. The data and analysis presented here must be regarded in this light. A definitive study of specular reflection will have to wait for improved instrumentation and techniques.

4. COMPARISON OF MICROWAVE BACKSCATTERING MODULATION WITH SURFACE SLOPE MODULATION

The DREP laser slope gauge offers us a unique opportunity to test models of microwave scattering from the ocean surface. Although the slope gauge is not co-located with the microwave beam so that a completely deterministic study of scattering (such as was done in the laboratory, Refs. 1, 2) is not possible, its close proximity (73 cm to the left when looking forward) means that modulations in microwave backscattering and in wave slope can be compared to provide some information on the validity of various scattering models.

We will first discuss how the microwave and slope data are analyzed. Microwave data consists of two separate channels, vv and hh, down-converted in two steps, from

9.13 GHz to 30 MHz to 20 KHz before it is recorded. To do detailed analysis, the recorded signals are down-converted again to 40 Hz by mixing with a signal roughly at 20 KHz from a frequency synthesizer. (A synthesizer is required since the recorded signal deviates slightly from 20 KHz from day to day). The signal is first low pass filtered at 300 Hz before being recorded onto a digital tape recorder at 512 Hz sampling rate. The low pass filtering minimizes high frequency fold-over. The digital tape is then analyzed by our PRIME 750 minicomputer. A 1024 point Fast Fourier Transform with a Hanning weighting is performed on 2 seconds of data every 0.5 sec. The spectrum typically shows a sharp peak at 40 Hz corresponding to the detuned signal and a broad peak Doppler shifted from 40 Hz, corresponding to the backscattered signal. For cases where the Doppler peak is clearly separated from the 40 Hz detuned signal, the spectrum is integrated from 50 Hz to 200 Hz to give the backscattered power as a function of time at 0.5 sec interval. For cases where the broad Doppler peak hovers around 40 Hz (which happens when the ship and the waves are moving at the same velocity), the portion of the sharp detuning peak above the broad Doppler peak is simply subtracted away before integration to yield the total power of the Doppler broadened signal. This process of integrating the spectrum to obtain the backscattered power is performed for both polarizations to produce the polarization ratio (hh/vv) as a function of time at 0.5 sec interval. The mean Doppler

shift as well as the width of the Doppler spectrum (at 10 dB below peak) can also be obtained by further processing for every spectrum, i.e., at 0.5 sec interval. To summarize, the radar signal is analyzed to obtain at 0.5 sec interval the following data: vv power, hh power, mean Doppler shift and width of Doppler spectrum of both polarizations. On the PRIME 750, a typical 10-minute run will take about 10 minutes computer time to analyze.

The laser slope gauge output is a voltage, which after calibration, becomes slope as a function of time. The slope signal analysis procedure is similar in some aspects to that of the radar. It is low pass filtered at 300 Hz and then recorded onto a digital tape at 512 Hz sampling rate. The tape is then analyzed on the PRIME 750 which performs a FFT on 2 sec. of data every 0.5 sec. The resulting spectrum of every 2 seconds of data is the slope spectrum. We recall that the slope power spectral density, S(f), is related to the waveheight power spectral density, Y(f), by:

$$S(f) = k^2 Y(f)$$

Let us assume that an X-band Bragg wave with wavelength and λ_B and wavenumber k_B is moving towards the ship with a relative velocity v. The laser beam will detect this Bragg wave as a disturbance with a "Bragg frequency" f_B where

$$f_B = v/\lambda_B \qquad (1)$$

If Bragg scattering theory is correct, then the microwave backscattered power, P, should be proportional to the waveheight spectral density at k_B in k - space, which is

proportional to the waveheight spectral density at f_B, in frequency space, i.e.,

$$P \propto Y(k_B) \propto Y(f_B) \propto S(f_B)$$

Thus modulation in backscattered power should be proportional to modulation of the slope spectrum at the "Bragg frequency" $f_B = v/\lambda_B$. In a relative dB scale, modulation in microwave backscattered power should be identical to modulation of the slope spectrum at the "Bragg frequency" within a constant additive factor.

The strategy of testing Bragg scattering theory is therefore quite simple in principle: Plot the microwave backscattered power (vv or hh) in a dB scale as a function of time as the ship passes through an internal wave field; select a narrow band around the "Bragg frequency" in the slope spectrum; integrate the slope power in this narrowband to obtain the "X-band-Bragg slope power" in a dB scale as a function of time. The 2 plots should be identical if Bragg scattering theory is correct.

To implement the strategy requires knowing where the "Bragg frequency" is and how wide a band we should integrate around it. From Eq.(1), the "Bragg frequency" is determined by the encounter velocity between the ship and the Bragg wave. We can determine the encounter velocity with increasing degree of accuracy and complexity by the following three methods. (1) The simplest thing to do is to assume the ship is moving with a constant velocity (which we obtain by averaging the ship's bow current meter reading

over a long period of time before the ship enters the internal wave field). We also assume the Bragg waves are either moving toward or away from the ship at their natural dispersion phase speed. The encounter velocity is simply the sum of the 2 velocities. Consequently, slope analysis is performed by setting a bandpass filter at a fixed frequency. (2) The ship, however, is not moving at constant velocity. In fact, the ship's bow current meter clearly shows it to be varying when the ship goes through an internal wave field. The ship's varying velocity can be taken into account in determining the encounter frequency with the Bragg wave. This corresponds to a slope analysis with a tracking filter that tracks with ship's varying velocity. This obviously complicates the data processing considerably. (3) Finally, we should realize that the Bragg wave phase speed is highly uncertain. The Bragg wave may be advected by a wind drift layer (typically ~ 3% wind speed); it may be advected by orbital speed of gravity waves; or it may actually be a locked component at the crest of a short gravity wave. At this point, just when it seems quite hopeless that we can determine the encounter velocity accurately, we should realize that the encounter velocity has already been measured -- by our Doppler radar! In fact, a little arithmetic will show that the "Ship-Bragg wave encounter frequency" is identical to the radar measured Doppler shift frequency. The slope analysis should

therefore involve a tracking filter that tracks with the radar measured Doppler frequency.

We note here that this analysis of the wave slope data assumes that the surface waves are moving along the direction of the line of sight of the radar, which is also the direction of the ships heading, since the radar responds only to Bragg waves moving in that direction. In a multidirectional situation it is possible that waves moving at an angle to the radar line of sight could contribute to slope data at the Bragg wave frequency even though they are not waves at the Bragg wavelength moving in the direction of the radar line of sight. The slope gauge is therefore capable of responding to waves approaching at a wider range of angles than the radar and this could affect comparisons between the radar backscatter and wave slope data bandpassed at the "Bragg frequency". This effect is considered negligible for the results reported here for several reasons. First, the internal waves were long-crested, the measurements were made while the ship was heading into the wave fronts (i.e., heading perpendicular to the long crests), and visual and video observations indicated that the short waves were aligned in the direction of the internal wave propagation, so that the configuration was essentially unidirectional. Second, since the major contributions to the relative speed of the short waves and the ship is from the ship speed, it can rather easily be seen that waves at an angle to the ship heading (and radar

line of sight) which would contribute slope data at the frequency of Bragg waves moving along the radar line of sight are waves having shorter wavelengths than the true Bragg waves. If the surface wave slope spectrum decreases with decreasing wavelength, this contributes further to the essentially unidirectional nature of these measurements. Thirdly, it is the modulations of wave slope and radar backscatter that are being compared here and not the absolute values. Regardless of the directional dependence of the slope spectrum, modulations of surface waves induced by internal waves are strongest in the surface wave components aligned with the internal wave direction, so that the modulations of interest tend to be concentrated in the unidirectional wave components.

The question of what bandwidth should be used in the slope analysis is quite interesting. Since the microwave Doppler bandwidth is time varying, we may be tempted to think that if slope power modulation does turn out to be identical to microwave power modulation, the bandwidth used in slope analysis should also be time varying. This reasoning is false on closer analysis. We can understand this more clearly by referring to Figure 7 which shows a schematic plot of the dispersion relation. In the ocean, due to the reasons mentioned above, the dispersion relation is no longer a sharp line. Rather, it is a band. If power is plotted vs. ω and k in a 3-D plot, the waveheight power spectral density is no longer a sheet, but a ridge. If the

Bragg scattering theory is correct, the radar measurement is a cut across this ridge at a constant k, with a finite Δk due to the finite spot size of the antenna. The cut at constant k across the ridge is in fact the Doppler spectrum of the radar signal. The slope spectral analysis (more accurately, the waveheight spectral analysis) is a cut across this ridge at a constant ω, with a finite $\Delta\omega$ to be determined. From the figure, we can see that comparing the integral along the constant k-cut (corresponding to microwave backscattered power, assuming Bragg scattering theory is valid) and the integral along the constant ω-cut (the Bragg slope power) is strictly speaking valid only when the dispersion relation is a line. When the dispersion relation becomes a band, the 2 integrals are integrating over 2 different regions (shown as shaded in the figure). However, it is easy to show that the 2 regions have the same area, to first approximation. For reasonably behaved power spectral density "ridges", the 2 integrals remain identical. From Figure 7, the answer to our original question should now be obvious. The $\Delta\omega$ should be chosen to correspond to the Δk of the radar footprint, i.e., $\Delta\omega = (d\omega/dk)\Delta k$, where $(d\omega/dk)$ is the slope of the dispersion relation.

Earlier, we asked whether the slope analysis bandwidth should vary when the width of the microwave Doppler spectrum varies with time. From Figure 7, it is clear that the Doppler spectrum changes width as a result of the dispersion relation band changing width, e.g., from the solid lines to

the dashed lines in Figure 7. The 2 integrals along constant k and constant ω remain equal. Hence, $\Delta\omega$ should remain constant because Δk of radar is constant, a reasoning which is not quite obvious without referring to Figure 7.

$\Delta\omega$, however, does not always remain constant. When the ship is going through an internal wave field, its velocity changes. Consequently the dispersion relation measured from the ship changes slope. As we mentioned above,

$\Delta\omega = (\frac{d\omega}{dk})\Delta k$ where $\frac{d\omega}{dk}$ = slope of dispersion relation, function of the ship's velocity

Hence, $\Delta\omega$ should track with the ship's velocity.

To summarize, the slope analysis is carried out to compute the "X-band" Bragg slope power. The "Bragg frequency" tracks the mean Doppler frequency as measured by our radar. The bandwidth for doing the slope power integration tracks with the ship's velocity as measured by the bow current meter.

The above analysis is performed also for the "L-band" Bragg slope power. In this case, we do not have a shipboard L-band radar to tell us the velocity of the L-band Bragg waves relative to the ship. For simplicity we assume that the relative speed of the ship and the L-band waves is the same as that for the X-band waves. This is equivalent to assuming that the X- and L-band waves are phase locked rather than dispersive, but we note here that the results in these cases turn out to be insensitive to which assumption is made because the dominant part of the relative velocity is

the ship's own velocity. The $\Delta\omega$ for L-band slope integration is taken to scale with wavelength, i.e., about 1/7 that of X-band.

The video signal has been analyzed as mentioned previously on a frame-by-frame basis to provide a semi-quantitative analysis of specular reflection. The video signal is a free-running indicator of the occurrence of specular points. The signal is first low-pass filtered at 5 Hz to remove the 60 Hz spikes (the TV field rate). It is then recorded at 512 Hz sampling rate on a digital recorder. The power is integrated over a 2 second interval every 0.5 msec. The logarithm of the power is taken before it is plotted out together with the rest of the signals.

Figure 8 shows a complete analysis of TRW run 71A (DREP 12-3). The top trace (in dots) is the current magnitude along ship track as measured by the ship's bow current meter. In an ambient sea without internal waves, this is the ship's velocity relative to the water mass, which may itself be moving, e.g., as in a tidal current. When an internal wave is present, its associated current (at 1 m below surface) will be superimposed onto the ship's velocity relative to water, as is apparent in this figure. The trace close to the current is the mean Doppler shift measured by the X-band radar, converted into velocity units. It shows the velocity of the microwave scatterer relative to the ship. The other traces, L-band Bragg slope, X-band Bragg slope, microwave backscattered power, polarization ratio,

video power, have been explained above. The starting and stopping of the run, the polarization of the microwave power displayed and the incidence angle of the microwave are indicated on the top of the figure. The direction of ship's heading, internal wave heading and wind vector are indicated in the circled figure.

The following observations can be made about Figure 8:

(i) The current trace shows 2 huge soliton-like internal wave "bumps". The current magnitude of the internal waves is as large as 70 cm/sec. This run is an example of a very strong internal wave.

(ii) "L-band" Bragg slope shows modulation peaks about 4.3 and 4.8 dB (peak over background, POB) at t = 90 sec and t = 435 sec whereas "X-band" Bragg slope shows slightly larger modulations of about 5.5 and 6.7 dB, respectively. This is contrary to most modulation theories where modulation of surface waves with X-band wavelength is generally expected to be a lot smaller than that in L-band.

(iii) Modulation in microwave backscattered power is a lot higher at the 2 modulation peaks, which are roughly 15 dB and 19 dB (POB). Otherwise, the rest of the microwave power trace is almost identical to that of the "X-band" Bragg slope trace. If the latter is overlaid on top of the former, it can be seen that even subtle changes in the background are reproduced

faithfully. This suggests that except during the modulation peaks, scattering may be predominantly Bragg scattering so that modulation in microwave power is identical to modulation in Bragg slope power, as explained previously. During the modulation peaks, another scattering mechanism other than Bragg scattering is responsible for the huge modulation.

(iv) The polarization ratio (hh/vv) trace stays roughly constant at about 0.25 (or -6 dB) except during the modulation peaks. This is consistent with Bragg scattering which predicts a ratio of -6.5 dB. During the modulation peaks, the polarization ratio approaches 1, suggesting specular reflection as the scattering mechanism.

(v) The video power trace confirms that specular reflection is indeed the scattering mechanism during the modulation peaks.

(vi) One prominent feature in the "X-band" Bragg slope is a modulation null of roughly 11 dB at t = 355 sec. This null is also present in the microwave power and to a lesser extent, in the "L-band" Bragg slope. Since this deep null is detected by the slope gauge and the radar which are independent instruments, it is real and not an instrument malfunction. Since we cannot correlate it with any special feature in the current, we suspect its origin is not solely hydrodynamic but surface slick induced.

(vii) The interpretation of the Doppler velocity is potentially the most interesting but also the most uncertain in this experiment. The reason for the uncertainty is that there is no other surface instrument that measures surface scatterer velocity to confirm what we think the radar is seeing. In our previous laboratory wavetank experiment[1,2] where a scanning laser slope gauge is available and where correlation between successive scans is possible, we found that electromagnetically, when the radar is seeing Bragg scattering, hydrodynamically, there can be three different kinds of Bragg scatterers. At low wind speed, the Bragg scatterer is a freely propagating Fourier component of a slightly rough surface on top of the wind drift layer, i.e., Doppler velocity = Bragg wave phase speed + wind drift layer velocity. At higher wind speed, the Bragg scatterer could be either (i) a turbulent patch moving at the velocity of the wind drift layer, i.e., Doppler velocity = wind drift layer velocity or (ii) a Fourier component of the parasitic capillaries which are phase-locked to the crest of short gravity waves, i.e., Doppler velocity = short gravity wave phase speed. At high wind speed, the mean Doppler velocity therefore lies somewhere between the wind drift layer velocity and the phase velocity of the dominant short gravity wave. We will now consider these two possibilities in Georgia Strait.

If the Bragg scatterer is a freely propagating Bragg wave, the offset between the Doppler velocity (as measured by the radar) and the current (as measured by the bow current meter) should be almost constant and quite predictable. This is because the offset would be equal to the Bragg wave intrinsic phase speed (which is constant) + the wind drift layer velocity (which is usually relatively small and almost constant if the wind field is almost constant). If the Bragg scatterer is a combination of turbulent patches and parasitic capillaries of short gravity waves, then the offset between the Doppler velocity and the current would be more variable. This is because the offset would be equal to the mean speed of turbulent patches and short gravity waves in the field of view. The speed of the turbulent patches would be the wind drift layer speed which is quite constant and predictable. The speed of short gravity waves (more precisely, its component along ship track) would be more variable due to variability in both magnitude and direction. Referring now to Figure 8, we can see that the offset between Doppler velocity and current meter output is far from constant. This rules out that scattering is entirely due to Bragg scattering from freely propagating Bragg waves. Closer examination will show that the microwave scatterers are moving towards the ship before and between the internal wave "bumps", but during the

"bumps" they actually change direction and move in the same direction as the ship and internal wave. To understand how this happens, we refer to Figure 9 which characterizes almost all the natural internal waves we have seen in Georgia Strait. Based on visual observations, an internal wave propagating from left to right is usually preceded by a dead calm region. Then comes a rough region. The demarkation between the calm and rough region is extremely sharp. From the demarkation line, short gravity waves appear to be growing in both wavelength and amplitude as they travel to the right, in the same direction as the internal wave, irrespective of wind direction. The short gravity waves may or may not break at some point, depending on whether the internal wave is strong enough. Further to the right, the short gravity waves grow longer but slowly die down in mag-nitude, becoming another dead calm region in front of the next cycle. In Run 71A as depicted in Figure 8, the wind is blowing at ~ 115° whereas the internal wave is traveling at 354°. Outside the internal wave bumps, the microwave scatterers, irrespective of origin, are naturally aligned with the wind direction, so that the net component along ship track is towards the ship. Inside the internal wave bumps, the short gravity waves as depicted in Figure 9 are now the microwave scatterers and so travel in the same direction as the

internal waves and ship. In fact, some of the sharp excursions downwards in the Doppler velocity can be clearly identified with the peaks in microwave power and peaks in polarization ratio. This closely agrees with our notion that specular reflection comes from short gravity waves breaking and surging forward. Outside the internal wave bumps, we have shown that polarization ratio indicates the scattering to be likely Bragg scattering. The Doppler velocity itself however cannot tell us whether the Bragg scatterers are (i) freely propagating or (ii) a combination of turbulent patches and parasitic capillaries on short gravity waves. If (i) is correct, the offset between the Doppler velocity and current traces should be equal to Bragg wave intrinsic phase speed (24 cm/sec) + wind drift velocity along ship track (3.8 m/sec x 0.03 x cos 66° = 5.1 cm/sec) = 29.1 cm/sec. This is not in bad agreement with the figure. However, (ii) cannot be ruled out. In fact, a combination of (i) and (ii) can also occur and cannot be ruled out. Measuring the offset between Doppler velocity and current can only definitively show whether (i) is incorrect, e.g., if the offset is 60 cm/sec, then it cannot possibly be due to a freely propagating Bragg wave on top of a wind drift layer in this low wind. A scanning laser slope gauge is definitely needed to shed more light on the identity of the Bragg scatterers.

(viii) In Run 71A in Figure 8, the demarkation between the calm region and rough region in the internal wave occurs at the divergence zone in the current. In all the other runs we have analyzed, this demarkation happens at the convergence zone. Just in case there is any doubt, we have analyzed Run 69 which is the ship going south one-half hour earlier and crossing the same internal waves. The demarkation between rough and calm regions still lie in the divergence zone. This peculiarity is still a mystery to us.

(ix) The "X-band" Bragg slope and "L-band" Bragg slope have been analyzed by tracking the "Bragg frequency" with the Doppler velocity of the radar. We have found that tracking with the current or a constant ship velocity does not make much difference. This implies that the effect of modulation is a lot greater than whatever error we may have incurred by using a slightly off Bragg frequency.

We will now examine TRW Run 81B which is an example of a very regular internal wave train (Figure 10, see Caponi et al, this issue, for a description of the conditions of TRW Run 81B). We can make the following observations:

(i) The agreement between the "X-band" Bragg slope and the microwave power is even more impressive in this example. When the slope trace is overlaid on top of the power trace, it can be seen that the only disagreement occurs around the null, where the noise

level of the slope gauge has been reached (and thus shows apparently higher level) and around the modulation peaks, where spikes from specular reflection occur in microwave power but not slope.

(ii) Comparison between the "L-band" slope and the X-band microwave power will show that while there is similarity, the agreement is nowhere as close. If the whole slope spectrum is integrated to give the mean square slope, it can be shown that the agreement between that and the microwave power is even worse. This shows that "X-band" Bragg slope, as we have defined it, is the proper descriptor of the surface to be compared with X-band microwave backscattering power.

(iii) The direction of travel between internal wave and the ship can be inferred from this figure. Referring back to Figure 9, we can see that the ship is first encountering the rough region, then the very sharp drop to the calm region. This means the ship is travelling against the internal wave.

(iv) The polarization ratio is again close to 0.25 (- 6dB) most of the time, indicating the presence of Bragg scattering. However, other than peaks that correspond to real power peaks, there are also spurious peaks in the modulation nulls. This is an artifact because both vv and hh signals are dropping close to noise level.

(v) The sharp demarkation lines between rough and calm regions occur at the convergence zone of the current in this run.

We will now examine TRW Run 112 (Figure 11). This is the case of a very weak internal wave in a calm sea. The following notable features are particular to this run:

(i) Even though the internal wave is weak, modulations in slope and microwave are nonetheless quite large, exceeding 20 dB in microwave. Again the noise floor in the slope masks the real bottoms of the modulation cycles.

(ii) If we examine carefully, almost every convergence point in the current corresponds to the sharp dividing line between the calm region and rough region of an internal wave cycle. The most prominent ones are pointed out by arrows in the figure.

(iii) The wind is extremely low (1.9 m/s), the sea very calm and the internal wave weak in this run. This would seem like a good candidate for observing freely propagating Bragg waves. Indeed, the Doppler velocity does show an almost constant offset of roughly 35 cm/sec from the current. A freely propagating Bragg wave would have a constant offset of roughly 28 cm/sec. The conjecture therefore seems quite reasonable.

5. CONCLUSIONS

With respect to specular reflection, we can draw the following conclusions:

(i) Specular reflection is highly significant at 20° incidence angle and not negligible at 40°.

(ii) Our relatively crude instrumentation, which was meant at first for detection purposes only, indicates that the specular points have large enough radius that they are no longer Rayleigh scatterers at X-band and therefore that the specular points observed by the optical system are also specular to the X-band microwave radar.

With regard to comparison of microwave scattering with slope data, we can draw the following conclusions:

(i) The good agreement of the X-band Bragg slope and the microwave backscattered power (when specular reflection is absent) shows that both the DREP slope gauge and the TRW radar are highly accurate instruments over their respective dynamic ranges. It also shows that Bragg scattering is a good description of microwave scattering when specular reflection is absent.

(ii) X- and L-band modulations (as evidenced by the respective Bragg slopes) are comparable in most runs. This is quite unexpected for most modulation theories.

(iii) In calm seas, lower signal level, but higher modulations are observed. These modulations are primarily due to Bragg scattering. In rougher seas,

the hydrodynamic modulations are generally lower. The microwave modulations can however be significantly enhanced by specular reflection.

(iv) Deep minima have been observed near current patterns, but with no obvious relationship to the current variations. These may be due to the presence of organic films on the surface.

(v) Under calm seas, weak internal waves can produce very strong modulations at X-band but weaker modulations at L-band (as evidenced by their respective Bragg slopes). Again, organic film is a likely non-hdyrodynamic factor that should be checked into in future experiments.

Our previous laboratory work[1,2] suggests that in addition to Bragg scattering, wedge diffraction from short gravity wave crests and specular reflection from breaking waves are important mechanisms for microwave backscattering at moderate incidence angles (20°-70°). Generally speaking, wedge diffraction and specular reflection enhance scattering by O(3-4 dB) and O(10 dB) respectively. To discern the wedge diffraction component in ocean scattering, a scanning laser slope gauge needs to be co-located with the radar so that a deterministic study can be carried out. In the present experiment, wedge diffraction may have enhanced the Bragg scattering background quite uniformly by a few dB. It may also be buried around or under the specular reflection events. (Wave crests tend to become sharp wedges just

before they break.) The confirmation of wedge scattering in the ocean will have to wait for a more precise measurement.

The video instrumentation in this experiment were meant to detect specular facets and provide a rough estimate of their sizes. A quantitative and accurate measurement of the radius of curvature distribution of specular points on the ocean surface will require improved instrumentation.

6. ACKNOWLEDGEMENT

The authors acknowledge Dr. Arthur Bruckheim and Dr. David Lewis of the Defense Advanced Research Project Agency (DARPA) for support of this project. We are indebted to Dr. Blyth Hughes and his associates at the Defence Research Establishment Pacific (DREP) of Canada for managing the overall experiment, for providing the ship platform and essential support, and for allowing us to use their laser slope gauge data. We also gratefully acknowledge Ken Beach and Ernie Hoover of TRW for their experimental support, and Dr. Robert Shuchman and Dr. David Lyzenga of ERIM and Dr. Henry Yuen and Dr. Daniel Hsu of TRW for many useful discussions.

7. REFERENCES

1. Daniel S. W. Kwoh and Bruce M. Lake, A Deterministic, Coherent, and Dual-Polarized Laboratory Study of Microwave Backscattering from Water Waves, Part I: Short Gravity Waves Without Wind, IEEE J. of Oceanic Engineering, Vol. OE-9, No. 5, December 1984, p. 291-308.

2. D. S. Kwoh and B. M. Lake, The Nature of Microwave Backscattering from Water Waves, in The Ocean Surface, Wave Breaking, Turbulent Mixing and Radio Probing, ed. by Y. Toba and H. Mitusyasu, D. Reidel Pub. Co., Dordrecht, Holland, 1985, p. 249-256.

3. G. R. Valenzuela, Theories for the Interaction of Electromagnetic and Oceanic Waves - A Review boundary-Layer Meteorology, 13, 1978, pp. 61-85.

APPENDIX

A specular point in the microwave antenna footprint will appear as a white dot or patch in the video recorded image. This is due to the fact that the finite-size diffused lamp has produced a finite-size virtual image in the convex surface around the specular point. From simple geometric optics, the magnification is given by

$$m = \frac{r}{r + 2 \cdot 0} \tag{1}$$

where r is the radius of curvature at the specular point and 0 is the object distance (i.e., lamp to water surface distance). The real length of the virtual image is given by

$$\ell_i = \ell_o \cdot m \tag{2}$$

where ℓ_i = length of the image and ℓ_o = length of the object, i.e., O.D. of the lamp.

The apparent length of the image in the video camera is then

$$\ell_{ia} = \ell_i \cdot \frac{0}{0 + i} = \frac{\ell_i}{1 + m} \tag{3}$$

where ℓ_{ia} = apparent length of the image in the video camera and i = distance of virtual image behind the water surface.

Combining Equations (1), (2) and (3), the radius of curvature can be expressed in terms of the apparent length of the image in the video camera as:

$$r = \frac{2 \cdot 0}{\left(\frac{\ell_o}{\ell_{ia}}\right) - 2} \tag{4}$$

We note here that if a projection lamp is used instead of a diffused lamp, the filament of the lamp will become the

object instead, the virtual image will be a point source, and no size differentiation will be possible. The intensity of the virtual image will be relatable to the radius, but the intensity measurement of a point is obviously less accurate than the size measurement of a patch in a video image.

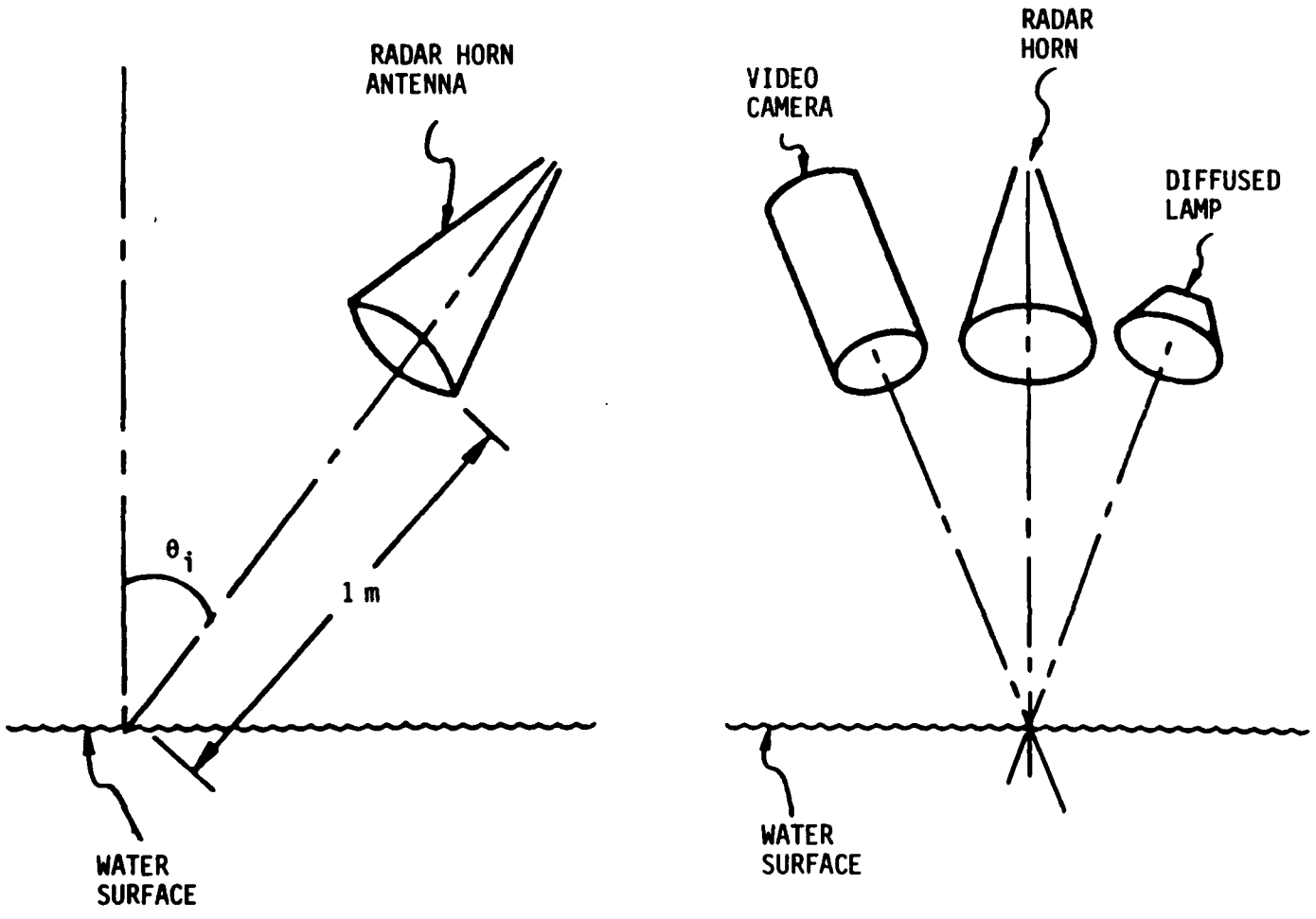

Figure 1. Schematic diagram of radar horn, lamp and video camera

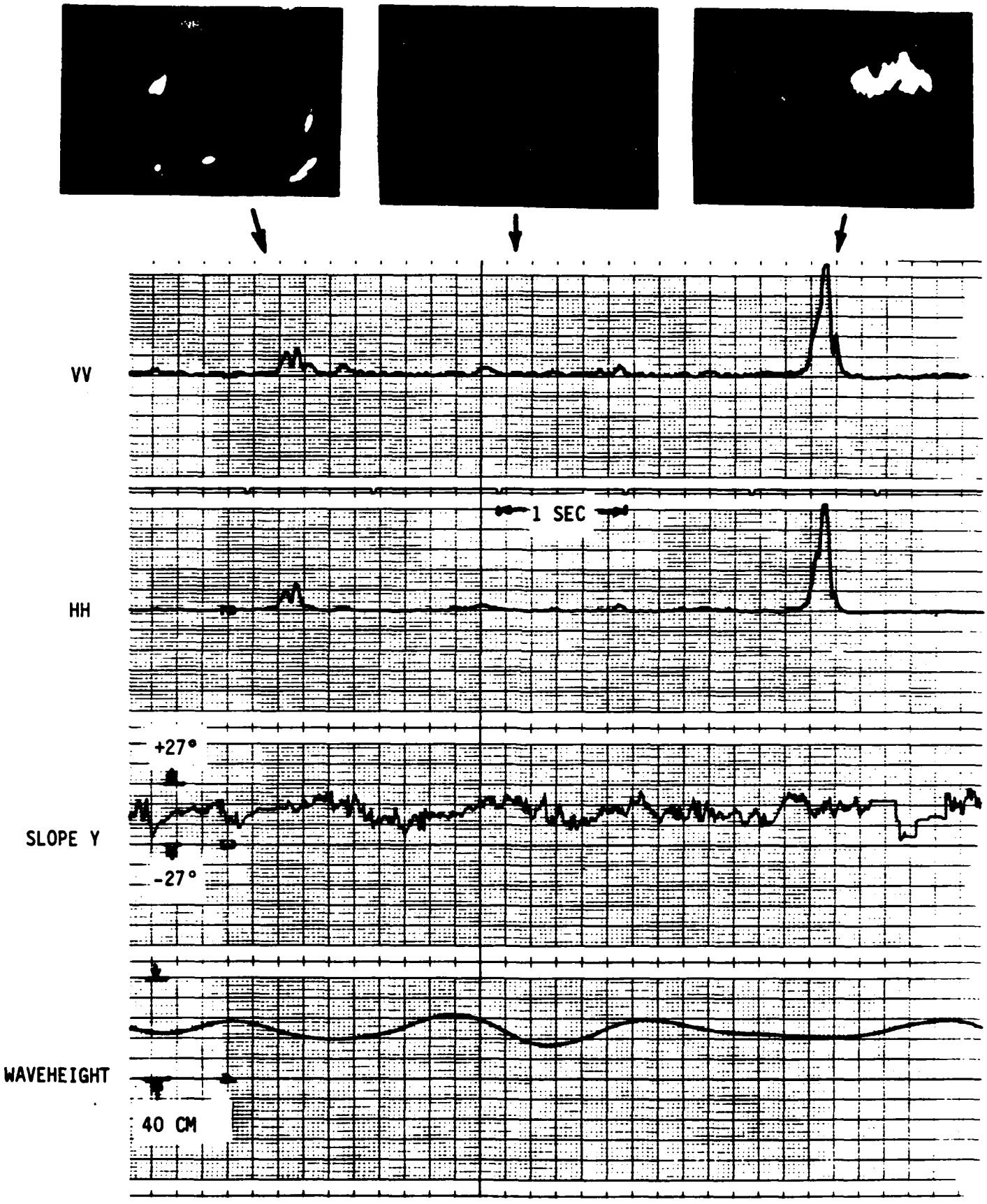

Figure 2. Video and microwave record of a specular reflection event.

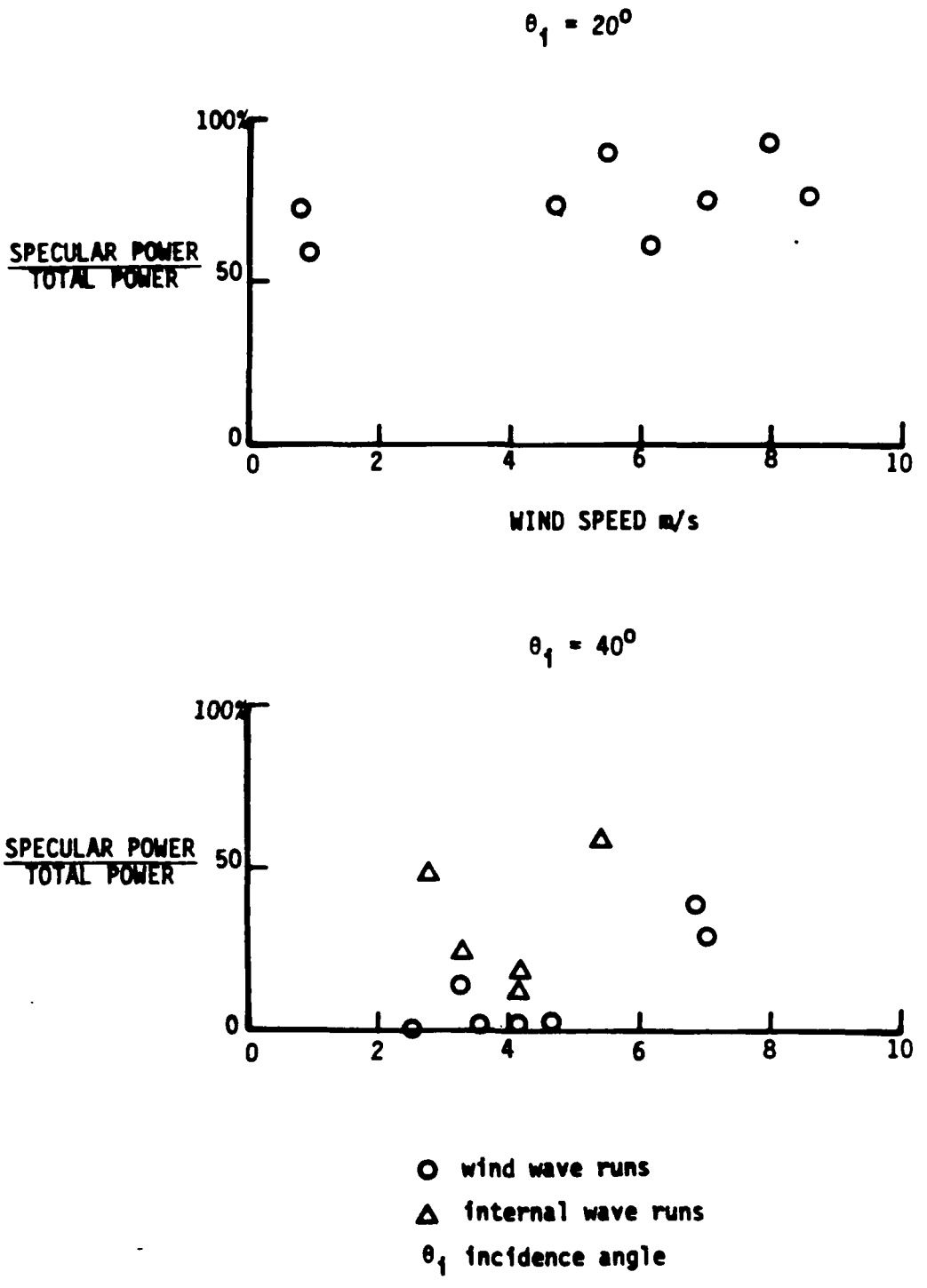

Figure 3. Specular reflection power/total backscattered power as a function of incidence angle and wind speed.

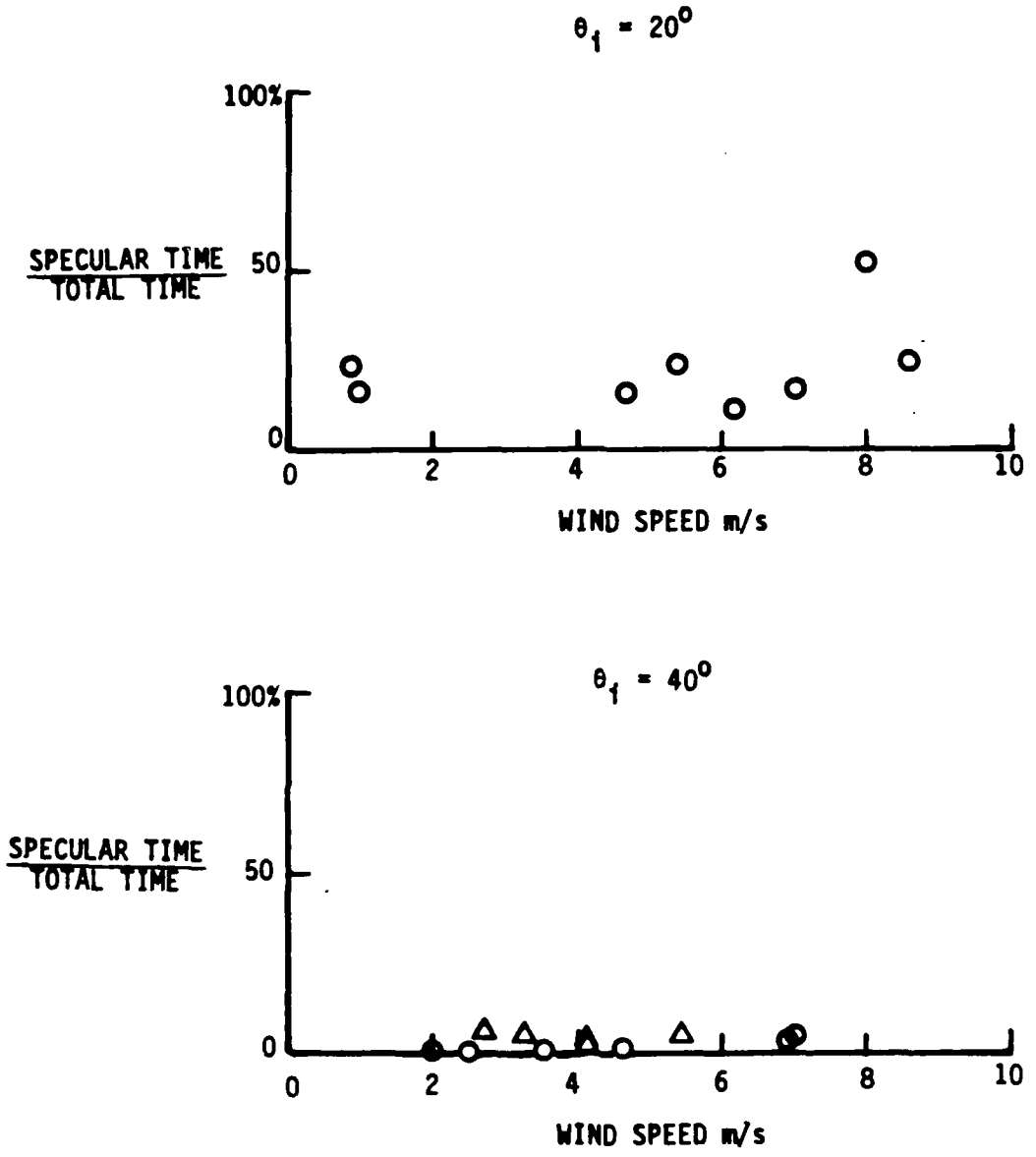

Figure 4. Fraction of time during which specular reflection occurs as a function of incidence angle and wind speed.

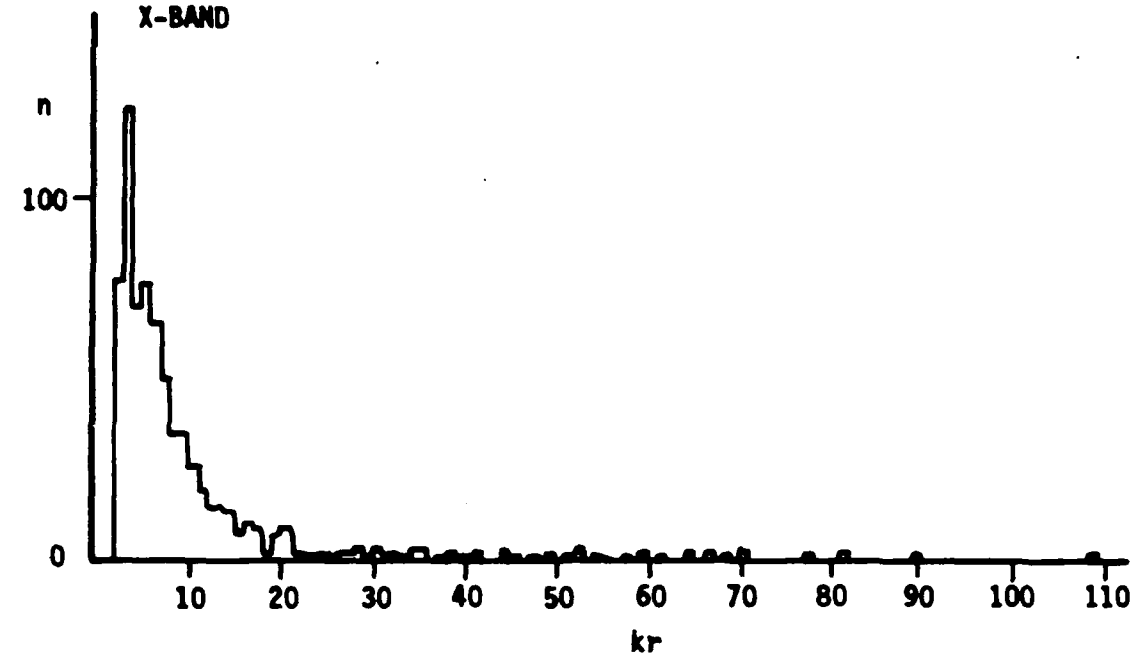

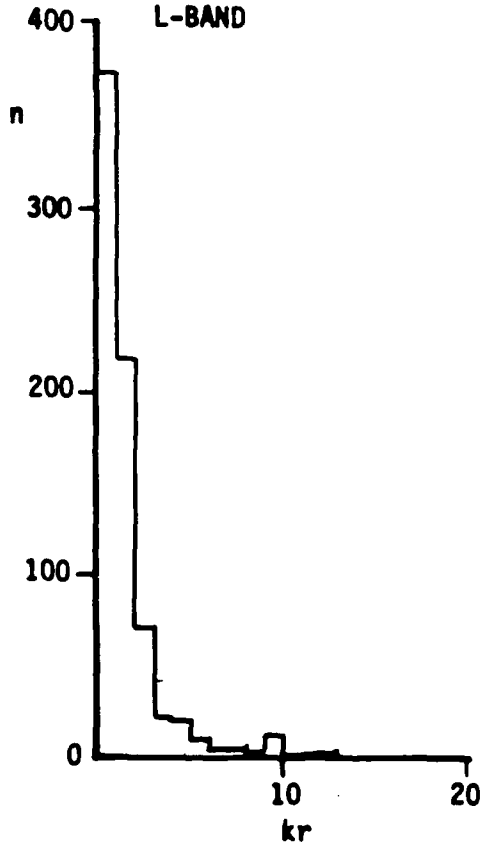

Figure 5. Size distribution of specular facets in TRW Run 81B as a function of kr in both X- and L-bands. 20 sec. of data; 40° incidence angle; 2.8 m/s wind speed.

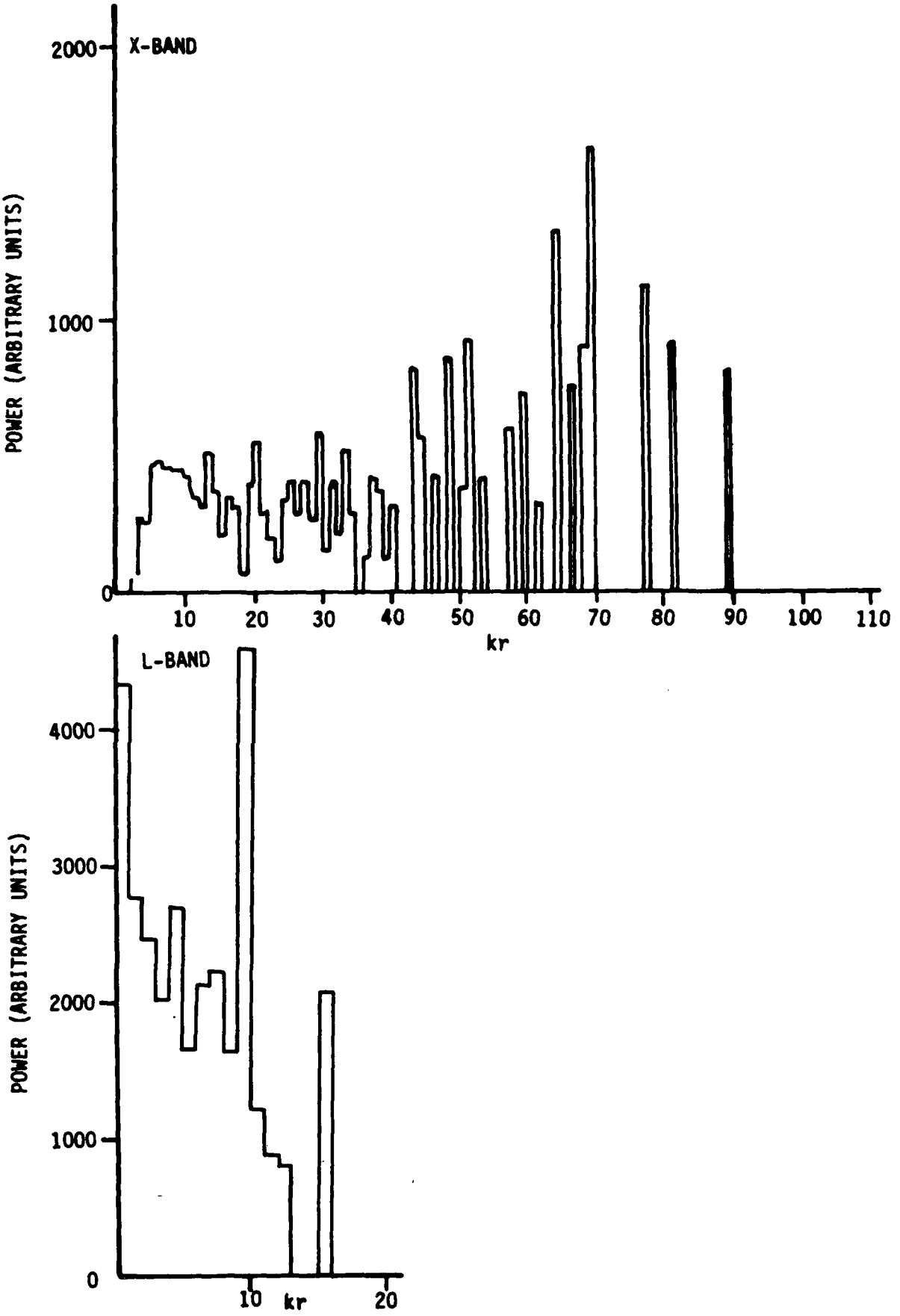

Figure 6. Power distribution of specular facets in TRW Run 81B as a function of kr in both X- and L-bands. 20 sec. of data; 40° incidence angle; 2.8 m/s wind speed.

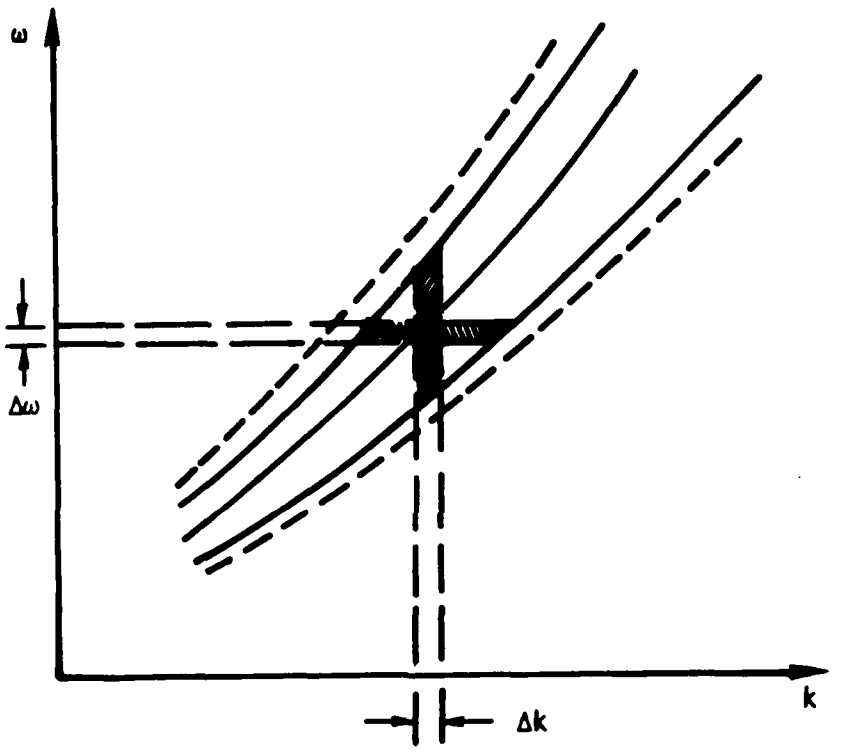

Figure 7. Schematic representation of dispersion relation of water waves in the ocean, showing relation of $\Delta\omega$ in slope analysis and Δk of radar footprint.

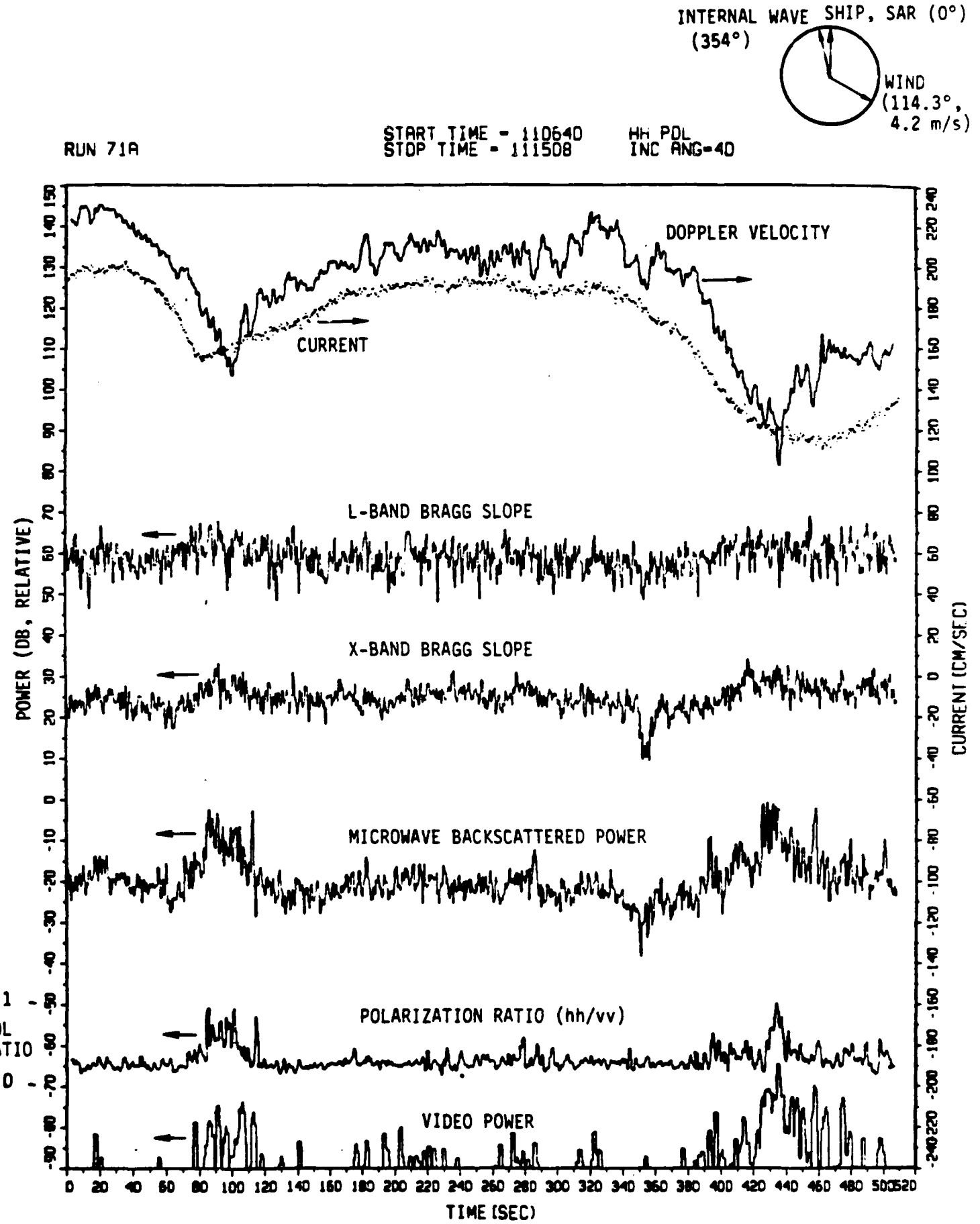

Figure 8. Complete analysis of TRW Run 71A (JOWIP 12-3). Incidence angle = 40°.

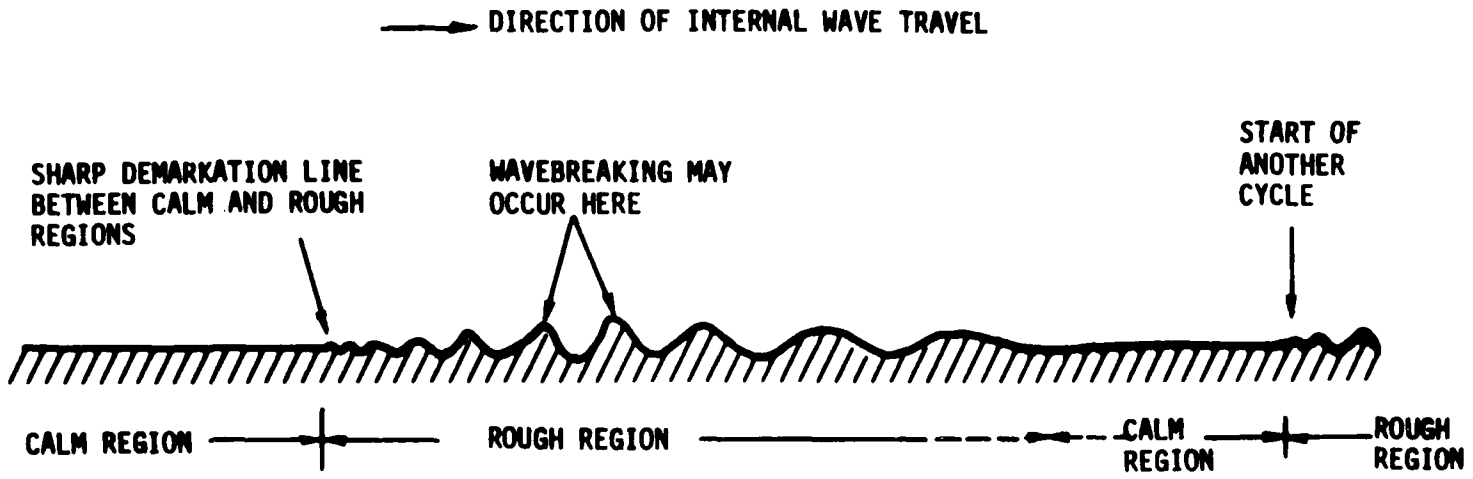

Figure 9. Surface wave manifestation of an internal wave cycle.

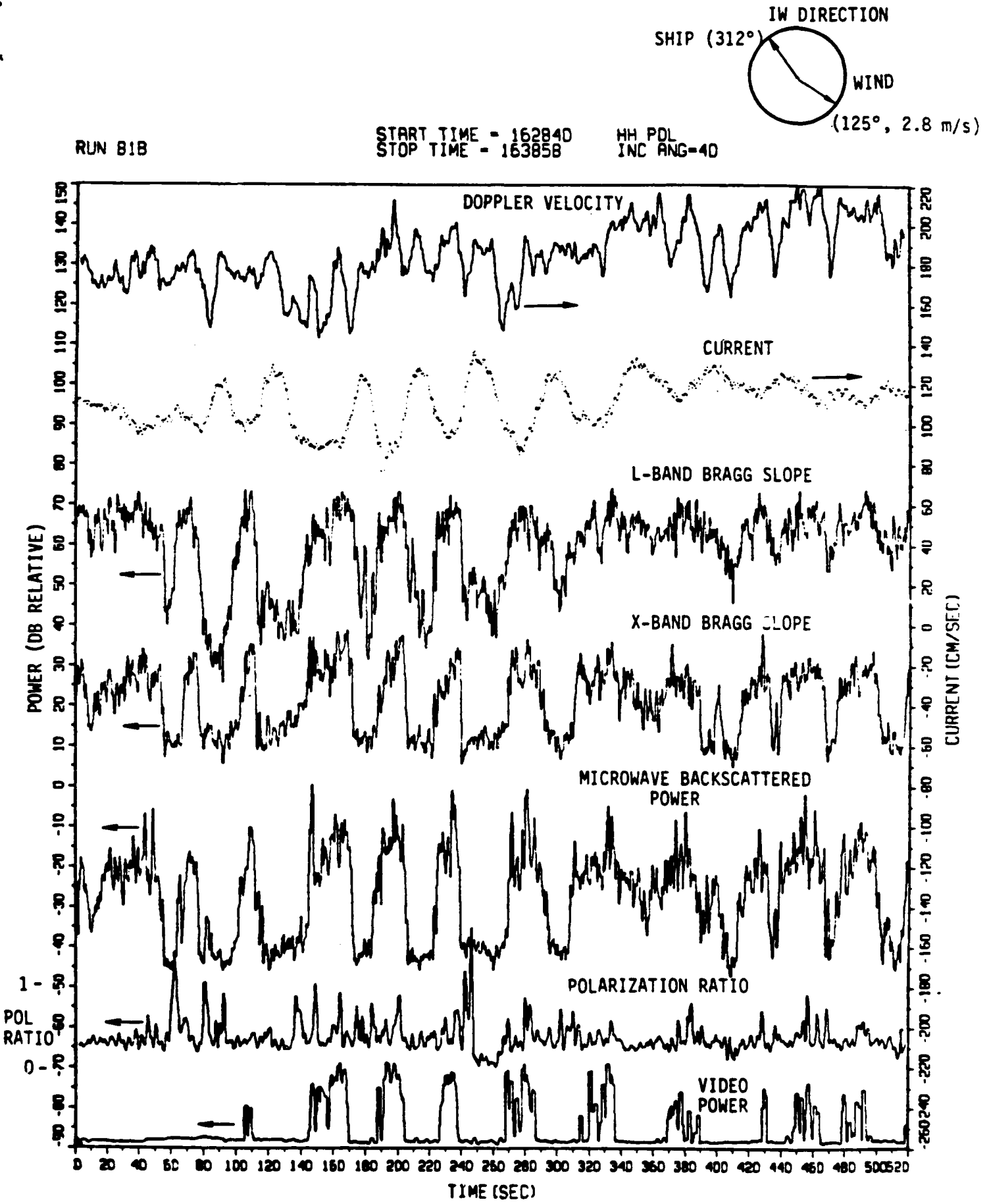

Figure 10. Complete analysis of TRW Run 81B . Incidence angle = 40°.

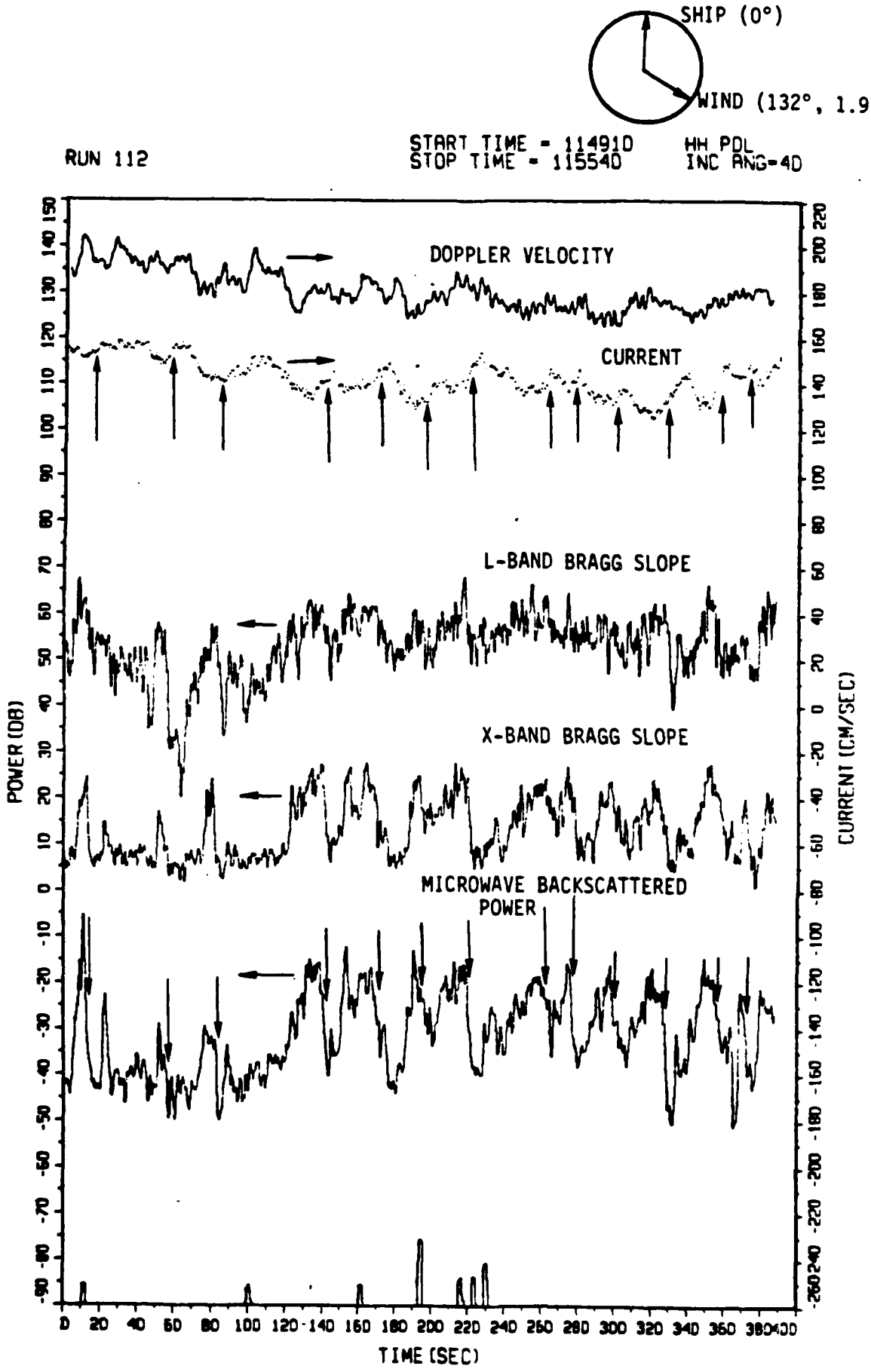

Figure 11. Complete analysis of TRW Run 112. Polarization ratio is not displayed because vv channel is out of tune. Incidence angle = 40°.